

BIOLOGICAL PATTERN FORMATION ON TWO-DIMENSIONAL SPATIAL DOMAINS: A NONLINEAR BIFURCATION ANALYSIS*

GERHARD C. CRUYWAGEN[†], PHILIP K. MAINI[‡], AND JAMES D. MURRAY[§]

Abstract. A tissue interaction model for skin organ pattern formation is presented. Possible spatially patterned solutions on rectangular domains are investigated. Linear stability analysis suggests that the model can exhibit pattern formation. A weakly nonlinear two-dimensional perturbation analysis is then carried out. This demonstrates that when bifurcation occurs via a *simple* eigenvalue, patterns such as rolls, squares, and rhombi can be supported by the model equations. Our nonlinear analysis shows that more complex patterns are also possible if bifurcation occurs via a double eigenvalue. Surprisingly, hexagonal patterns could not develop from a primary bifurcation.

Key words. pattern formation, nonlinear bifurcation analyses, tissue interaction

AMS subject classification. 92

PII. S0036139996297900

1. Introduction. The development of a complex multicellular organism from a single initial cell is one of the most intriguing phenomena in the natural sciences. Mathematical models have been widely used to investigate how embryonic cells become organized in a collection of spatial structures and forms, a process called morphogenesis. Particular examples include the formation of structure, such as hair, scales, feathers and glands, on the vertebrate skin. The skin is composed of two basic layers, the epidermis and the dermis, which are separated by a thin layer of tissue called the basal lamina. The vast majority of models proposed so far for morphogenesis in the skin have focused on pattern formation in one or other of these layers.

Two widely used models for pattern formation are reaction-diffusion models (Turing 1952) and mechanochemical models (see Murray, 1989 for review). Models of both types have been proposed as possible mechanisms underlying the formation of patterns in either the dermal or epidermal layers of skin.

Experimental evidence (refer to Murray and Cruywagen (1994) for references) indicates, however, that there is a strong coupling between these two layers. Nagorcka, Manoranjan, and Murray (1987) introduced the first tissue interaction models based on coupled reaction-diffusion systems. Shaw and Murray (1990) used a coupled mechanochemical system to model tissue interaction. Both papers demonstrated that a complex spatial pattern could arise from the coupling of two systems which could, individually, give rise to pattern.

These initial tissue-interaction models have the common property of being able to produce patterns independently in the dermis and the epidermis. Biologically, however, the dermis cannot produce coherent patterns without the presence of the epidermis and vice versa. Cruywagen and Murray (1992) subsequently proposed a

*Received by the editors January 31, 1996; accepted for publication (in revised form) July 24, 1996.

<http://www.siam.org/journals/siap/57-6/29790.html>

[†]Sea Fisheries Research Institute, Private Bag X2, Rogge Bay, 8012 Cape Town, South Africa. The research of this author was supported by the South African Foundation for Research Development.

[‡]Centre for Mathematical Biology, Mathematical Institute, 24–29 St. Giles', Oxford, England OX1 3LB (maini@maths.ox.ac.uk).

[§]Department of Applied Mathematics FS-20, University of Washington, Seattle, WA 98195. The research of this author was supported in part by U.S. National Science Foundation grant DMS9500766 and U.S. National Institutes of Health grant 2P41 RR01243-12.

model in which two mechanochemical-type systems can produce patterns only if they are coupled. Their model is more realistic, biologically, encompassing the crucial components involved in tissue interaction. It is one of the more realistic models proposed thus far, since it includes mechanochemical features such as cell adhesion molecules (CAMs) and tissue interaction via cell-cell signalling.

Here we show with the aid of a bifurcation analysis that on a two-dimensional domain, this model not only gives rise to the usual simple patterns but can also exhibit vastly complex patterns which are sometimes seen in nature.

We describe the full model in section 2. As this is a very complicated system we derive a reduced form of the model which retains the key features of the full model. The reduced model, consisting of a parabolic equation coupled with an elliptic equation, admits the usual basic uniform steady-state solution. In the appropriate parameter space, determined by the linear analysis presented in section 3, this steady state can be driven unstable and eventually evolves into a new nonhomogeneous steady-state solution. To get a better idea of the patterns possible, we examine the system analytically and numerically in the vicinity of the bifurcation point.

Although pattern formation models in one dimension have been extensively studied using bifurcation analysis, the complexity of the analysis on two-dimensional domains is such that only a few studies have been carried out. Maini and Murray (1988), analyzed the nonlinear behavior of a single equation model in the vicinity of a simple eigenvalue. Ngwa and Maini (1995) investigated spatio-temporal patterns in a mechanical model using analytic and numerical techniques. Recently, a number of papers have analyzed the pattern formation properties of reaction-diffusion models in two dimensions (see Benson, Maini, and Sherratt (1997) and references therein). Such detailed studies do not exist for mechanochemical models, and our purpose here is to extend the analysis to such models.

We consider our tissue interaction model on a two-dimensional rectangular domain, taken to model skin. This system bifurcates to spatial pattern at either a simple eigenvalue, as is the case for the one-dimensional problem, or at a multiple eigenvalue. Of particular mathematical interest is the bifurcation problem from a multiple eigenvalue, since, as far as we know, this has not been widely studied in tissue interaction models. The linear and nonlinear analyses of the equations in such cases are naturally much more involved. Instead of only single mode patterns evolving, various modes can interact to produce mixed mode solutions. In these cases more complicated but also biologically realistic patterns can evolve due to the interaction of different modes of pattern. However, the analysis is also much more complicated. In this paper, specific attention is given to degenerate cases in the bifurcation analysis.

The bifurcation analysis gives a good indication of the type of patterns one could expect for various parameter ranges. We look specifically at rolls, rhombi, hexagons, and more complicated mixed mode patterns, since these are very common in nature.

In section 4 a weakly nonlinear multiple time-scale bifurcation analysis is used to examine the type of patterns that can arise. Specific examples are considered in section 5. For each, a bifurcation diagram is plotted and the solution predicted from the nonlinear analysis is compared with numerical simulations of the model equations.

2. The mathematical model. The model we consider here is a simplified version of the original continuum tissue interaction model of Cruywagen and Murray (1992). We briefly describe this model and refer the reader to the original paper for full details. By retaining only the most important components it is easier to examine the specific role played by different biological processes in the formation of pattern.

The model consists of two submodels, one for describing dermal cell movement and one for describing epithelial sheet deformation. These two submodels are coupled via tissue interaction between the dermal and epithelial skin layers.

The epithelial sheet is modeled as a two-dimensional, visco-elastic continuum (see, for example, Murray and Oster (1984); Murray (1989)). Since the system is in a low Reynold’s number regime, we assume that the visco-elastic and cell traction stresses within the epidermis are balanced by the external body forces. Assuming that the field variable $\mathbf{u}(\mathbf{x}, t)$ represents the displacement at time t of a material point in the epithelial layer which was initially at position \mathbf{x} , the force balance equation takes the form

$$(2.1) \quad \nabla \cdot \left\{ \overbrace{\frac{E}{1+v} [\boldsymbol{\varepsilon} - \beta_1 \nabla^2 \boldsymbol{\varepsilon} + v'(\theta - \beta_2 \nabla^2 \theta) \mathbf{I}]}^{\text{elastic stress}} + \underbrace{\mu_1 \frac{\partial \boldsymbol{\varepsilon}}{\partial t} + \mu_2 \frac{\partial \theta}{\partial t} \mathbf{I}}_{\text{viscous stress}} + \underbrace{\frac{\tau s^2(n)}{(1 + cs^2(n)) \mathbf{I}}}_{\text{traction}} \right\} = \underbrace{\rho \mathbf{u}}_{\text{body forces}},$$

where $\boldsymbol{\varepsilon} = (\nabla \mathbf{u} + \nabla \mathbf{u}^T)/2$ is the strain tensor, $\theta = \nabla \cdot \mathbf{u}$ the dilation, T denotes the transpose, and \mathbf{I} is the unit tensor. The parameter $v' = v/(1 - 2v)$ where v is Poisson’s ratio, E is Young’s modulus, and, μ_1 and μ_2 are the shear and bulk viscosities, respectively (Landau and Lifshitz (1970)).

The strength of the long-range elastic stresses are measured by β_1 and β_2 which are both positive (see Murray (1989) for a discussion of these terms). The epidermis is attached to the basal lamina with adhesion tethers; ρ reflects the strength of these attachments. The epithelial sheet exerts active traction which we assume depends on a signal chemical s , which diffuses from the dermis into the epidermis, thus introducing dermal to epidermal interaction. This active traction is modeled in the usual way by a switch function (see, for example, Murray and Oster (1984)), with τ measuring the magnitude of the switch and c the abruptness of the switch.

An epithelial cell conservation equation relates the epidermal cell density $N(\mathbf{x}, t)$ to the displacement \mathbf{u} . Since the only contribution to cell flux is convection, the equation is simply

$$(2.2) \quad \frac{\partial N}{\partial t} = -\nabla \cdot \overbrace{N \frac{\partial \mathbf{u}}{\partial t}}^{\text{convection}}.$$

For modeling dermal morphogenesis a chemotaxis equation, related to the cell-chemotaxis model of Oster and Murray (1989) and based on the *morphoregulator hypothesis* of Edelman (see, for example, Edelman (1986)) is used. According to this hypothesis, skin organ morphogenesis is controlled by cell-cell adhesion mechanisms mediated by CAMs. Chemical modulation can have a marked effect on the binding rates and binding strengths of CAMs (Grumet and Edelman (1988)), so we assume that a chemical signal concentration e , diffusing from the epidermis into the dermis, is responsible for CAM expression, thus introducing epidermal to dermal interaction. The conservation equation for dermal cell density, $n(\mathbf{x}, t)$, takes the form

$$(2.3) \quad \frac{\partial n}{\partial t} = \overbrace{\nabla \cdot D \nabla n}^{\text{diffusion}} - \overbrace{\nabla \cdot n \alpha \nabla e}^{\text{chemotaxis}},$$

where D is the coefficient of random diffusion and α is the chemotactic factor. Both parameters are positive.

We assume, reasonably, that the chemicals e , diffusing from the epidermis to the dermis, and s , diffusing from the dermis to the epidermis, are produced by the cells in the epidermal and dermal layers, respectively. As a first approximation we express the chemical concentrations as

$$(2.4) \quad e(N) = k_e N, \quad s(n) = k_s n,$$

where k_e and k_n are positive constants. Note that the original system as proposed by Cruywagen and Murray (1992) is much more involved, since they actually used four reaction-diffusion equations to model the chemical dynamics (two equations for each layer).

The system (2.1), (2.2), (2.3), and (2.4) constitutes the field equations of our tissue-interaction model. The full system is extremely complex but by making a few reasonable biological assumptions it can in fact be reduced to two coupled nonlinear equations, thus making it more amenable to analysis, while still retaining the essential biological features of the full model.

It is reasonable to assume that the epithelial viscosity parameters μ_1 and μ_2 are negligibly small compared with the other parameters in the equation, so we set them to zero. Note that taking the divergence of the epidermal tensor equation (2.1), reduces it to a scalar dilation equation in θ . Since the strains are very small in the epithelial sheet during the initial stages of morphogenesis, we can also apply the usual small strain assumption to equation (2.2). After linearizing about the steady state $N = 1$ a linear relationship $N = 1 - \theta$ between epidermal cell density and dilation is obtained. This relationship, along with equations (2.4), is substituted into equations (2.1) and (2.3) to give a simplified caricature model.

The reduced model involves only an elliptic equation in epithelial dilation θ and a parabolic equation in dermal cell density, n , namely,

$$(2.5a) \quad \nabla^2 \theta - \beta \nabla^4 \theta + \nabla^2 \left\{ \frac{\tau n^2}{1 + cn^2} \right\} = \rho \theta,$$

$$(2.5b) \quad \frac{\partial n}{\partial t} = D \nabla^2 n - \nabla \cdot (n \nabla \alpha (1 - \theta)),$$

where k_s^2 has been incorporated into the parameters τ and c , k_e has been included in the parameter α , $\beta = \beta_1 + \beta_2$, and β , τ , and ρ have been divided by $(1 + v')$.

The specific tissue geometry considered is idealized as a rectangular domain \mathbf{B} with dimensions (L_x, L_y) , and we assume zero-flux boundary conditions

$$(2.6) \quad (\boldsymbol{\eta} \cdot \nabla)n = 0, \quad (\boldsymbol{\eta} \cdot \nabla)\theta = 0, \quad (\boldsymbol{\eta} \cdot \nabla^3)\theta = 0 \quad \text{on } \partial \mathbf{B},$$

where $\boldsymbol{\eta}$ is the unit normal vector on the boundary $\partial \mathbf{B}$ of the domain \mathbf{B} . This ensures that the dermal and epidermal cell densities are conserved.

3. Linear stability analysis. Here we examine the two-dimensional tissue interaction problem linearized about the biologically realistic steady state $\theta = 0$, $n = 1$,

$$(3.1a) \quad \rho \theta = \nabla^2 \theta - \beta \nabla^4 \theta + P \nabla^2 n,$$

$$(3.1b) \quad \frac{\partial n}{\partial t} = D \nabla^2 n + \alpha \nabla^2 \theta,$$

where

$$P = \frac{2\tau}{(1+c)^2}.$$

By looking for solutions of the form $e^{i\mathbf{k}\cdot\mathbf{x}+\lambda t}$ we find that the dispersion relation takes the form

$$\lambda(k^2) = -\frac{c(k^2)}{b(k^2)},$$

where

$$\begin{aligned} b(k^2) &= \beta k^4 + k^2 + \rho, \\ c(k^2) &= \beta D k^6 - (\alpha P - D)k^4 + \rho D k^2. \end{aligned}$$

It is easy to determine the conditions under which $c(k^2) < 0$ and hence the parameter space in which the linear analysis predicts spatially nonhomogeneous solutions. We require that

$$\alpha P - D > 0 \quad \text{and} \quad (\alpha P - D)^2 > 4\beta\rho D^2.$$

From this it follows that increasing the effect of the interaction mechanism, which is achieved by increasing either α or P , destabilizes the system from its homogeneous steady state. We choose the chemotactic factor α as our bifurcation parameter and define α_c as the critical value at which the linear homogeneous steady state loses stability. For $\alpha > \alpha_c$ we have a range of unstable eigenvalues (k_-^2, k_+^2) where

$$k_{\pm}^2 = \frac{(\alpha P - D) \pm \sqrt{(\alpha P - D)^2 - 4\beta\rho D^2}}{2\beta D}.$$

At the critical point where $\alpha = \alpha_c$,

$$(\alpha_c P - D)^2 = 4\beta\rho D^2,$$

while the critical eigenvalue

$$k_c^2 = \frac{\alpha_c P - D}{2\beta D}.$$

Solutions to the linear system (3.1) satisfying the boundary conditions (2.6) are

$$(3.2) \quad \mathbf{w}(\mathbf{x}, t) = \begin{pmatrix} \theta \\ n \end{pmatrix} = \sum_{\tilde{\phi}, \tilde{\psi}} p_f(\tilde{\phi}, \tilde{\psi}) \begin{pmatrix} 1 \\ M(k^2) \end{pmatrix} e^{\lambda(k^2)t} \cos \phi x \cos \psi y,$$

where the discrete wavevectors $\mathbf{k} = (\phi, \psi)^T$ are members of the sequence

$$(3.3) \quad \phi = \frac{\tilde{\phi}\pi}{L_x}, \quad \psi = \frac{\tilde{\psi}\pi}{L_y}, \quad \tilde{\phi}, \tilde{\psi} = 0, 1, 2, \dots,$$

and

$$M(k^2) = \frac{-\alpha k^2}{\lambda(k^2) + D k^2}.$$

Each $p_f(\tilde{\phi}, \tilde{\psi})$ is determined by a Fourier transform of the initial conditions.

The spatially heterogeneous solution that emerges for large time (from the linear analysis), then, is the sum of the terms, or modes, in (3.2) corresponding to the *mode pairs* $(\tilde{\phi}, \tilde{\psi})$ for which

$$\lambda \left(\left(\frac{\pi \tilde{\phi}}{L_x} \right)^2 + \left(\frac{\pi \tilde{\psi}}{L_y} \right)^2 \right) > 0.$$

In the remainder of this section we shall be concerned mainly with examples for which the uniform steady state is unstable to modes corresponding to only one of the discrete eigenvalues, say k_c^2 . Depending on the domain size, k_c^2 could be either a simple or a multiple eigenvalue. If k_c^2 is a multiple eigenvalue, one or more of the mode pairs $(\tilde{\phi}, \tilde{\psi})$ from the above sequence (3.3) satisfies the expression

$$k_c^2 = \left(\frac{\tilde{\phi}\pi}{L_x} \right)^2 + \left(\frac{\tilde{\psi}\pi}{L_y} \right)^2.$$

For the square domain, $L_x = L_y$, some examples of mode pairs corresponding to a simple eigenvalue are $\{(1, 1)\}, \{(2, 2)\}$. Double eigenvalues correspond to the sets of mode pairs $\{(0, 1), (1, 0)\}, \{(0, 2), (2, 0)\}$, while a triple eigenvalue would, for example, correspond to $\{(5, 5), (1, 7), (7, 1)\}$ and so on.

A large variety of linear patterns could develop from various sets of allowable modes. Since the dermal cell density solution n differs from the epithelial dilation θ only by the constant factor $M(k_c^2)$, its solution is qualitatively similar to that of θ . For simplicity we shall therefore only examine the dilation solutions θ of the linear problem (3.1).

In general, single mode pair solutions give rise to rhombic spatial patterns, since the linear time independent solution which emerges is of the form

$$(3.4) \quad \theta(\mathbf{x}) = \cos \phi x \cos \psi y,$$

where $\mathbf{k}_c = (\phi, \psi)^T$ is the discrete wavevector satisfying the zero-flux boundary conditions (2.6). Note that the solution (3.4) has been scaled so that $\theta(0, 0) = 1$.

Expression (3.4) can be rewritten, in terms of polar coordinates (r, ϑ) , as

$$(3.5) \quad \theta(r, \vartheta) = \frac{\cos\{\kappa r \cos(\vartheta - \frac{1}{2}\varphi)\} + \cos\{\kappa r \cos(\vartheta + \frac{1}{2}\varphi)\}}{2},$$

where

$$(3.6) \quad \kappa = \sqrt{\phi^2 + \psi^2} = \sqrt{k_c^2}, \quad \varphi = 2 \arccos \left(\phi / \sqrt{k_c^2} \right).$$

It is now easy to see that φ represents the rhombic angle of the solution and that the solution is indeed invariant under a rhombic rotation; that is,

$$\theta(r, \vartheta) = \theta(r, \vartheta + \pi) = \mathcal{R}\theta(r, \vartheta) = \theta(r, \vartheta),$$

where \mathcal{R} is the rhombic operator.

If $\varphi = \pi/2$ or $\varphi = 3\pi/2$, then $\phi = \psi$ and a square or chessboard-type pattern results. This is a special case of the rhombic pattern, and the solution is square rotationally invariant.

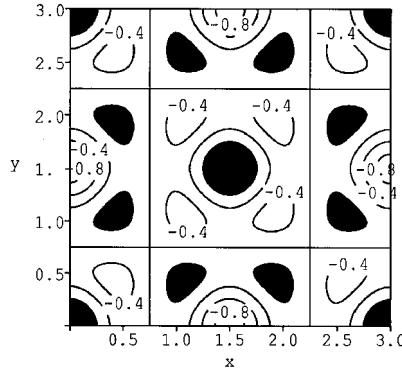


FIG. 1. The linear double mode solution corresponding to the mode pairs (2, 6) and (6, 2) plotted on the square domain (3, 3); see expression (3.4). Here $\alpha = \beta = \frac{1}{2}$. Regions where the solution is larger than 0.8 are shaded.

The simplest nonhomogeneous pattern possible on the two-dimensional rectangular domain is the roll, which occurs when either $\phi = 0$ or $\psi = 0$ in the rhombic solution (3.4). The roll is invariant under a rotation of π .

All the linear patterned solutions arising from a simple eigenvalue, as discussed above, tessellate the plane, since they satisfy

$$\mathbf{\Gamma}(\mathbf{x} + j\boldsymbol{\omega}_1 + l\boldsymbol{\omega}_2) = \mathbf{\Gamma}(\mathbf{x}),$$

where $\mathbf{\Gamma} = (n, \theta)^T$ is the solution of the system, j, l are integers and $\boldsymbol{\omega}_1, \boldsymbol{\omega}_2$ are appropriately chosen independent vectors. Patterns corresponding to multiple eigenvalues are not usually tessellations of the plane.

A much richer class of mixed mode patterns does, however, exist. For example, when we have a double eigenvalue k_c^2 , with the two corresponding wavevectors, say $(\phi_1, \psi_1)^T$ and $(\phi_2, \psi_2)^T$, satisfying the zero-flux boundary conditions (2.6), two rhombic patterns interact; thus

$$(3.7) \quad \theta(\mathbf{x}) = \alpha \cos \phi_1 x \cos \psi_1 y + \beta \cos \phi_2 x \cos \psi_2 y,$$

where α and β are real numbers so that $\alpha + \beta = 1$. (This scales the time-independent solution so that $\theta(0, 0) = 1$.) Specifically, if we consider a square domain of dimensions (3, 3) and isolate the unstable eigenvalue $k_c^2 = 40\pi^2/9$, then the corresponding unstable mode pairs are (2, 6) and (6, 2). The time-independent solution to the linear problem, where $\alpha = \beta = 1/2$, is as illustrated in Figure 1.

Mixed mode patterns can vary considerably depending on the modes interacting. There is, however, a simple pattern tessellating the plane that can be generated by two interacting modes. When the two wavevectors are

$$(3.8) \quad \begin{pmatrix} \phi_1 \\ \psi_1 \end{pmatrix} = \begin{pmatrix} \kappa \\ \sqrt{3}\kappa \end{pmatrix}, \quad \begin{pmatrix} \phi_2 \\ \psi_2 \end{pmatrix} = \begin{pmatrix} 2\kappa \\ 0 \end{pmatrix},$$

or

$$(3.9) \quad \begin{pmatrix} \phi_1 \\ \psi_1 \end{pmatrix} = \begin{pmatrix} \sqrt{3}\kappa \\ \kappa \end{pmatrix}, \quad \begin{pmatrix} \phi_2 \\ \psi_2 \end{pmatrix} = \begin{pmatrix} 0 \\ 2\kappa \end{pmatrix},$$

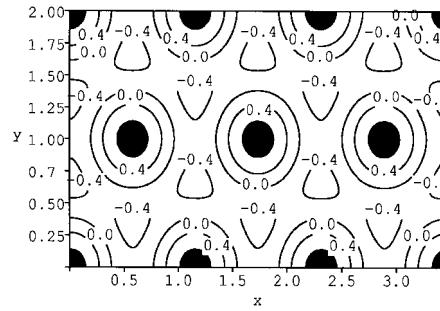


FIG. 2. Contour graph of the linear hexagonal pattern corresponding to the mode pairs $(6, 2)$ and $(0, 4)$ plotted on the rectangular domain $(2\sqrt{3}, 2)$; see expression (3.9). Regions where the solution is larger than 0.8 are shaded.

and $\alpha = 2/3$, $\beta = 1/3$, then a hexagonal pattern results. With wavevectors as in (3.8) the solution can be written as

$$(3.10) \quad \theta(\mathbf{x}) = \frac{\cos \kappa(\sqrt{3}y + x) + \cos \kappa(\sqrt{3}y - x) + \cos 2\kappa x}{3},$$

which, in terms of polar coordinates (r, ϑ) , is

$$\theta(\mathbf{x}) = \frac{\cos\{2\kappa r \sin(\vartheta + \frac{\pi}{6})\} + \cos\{2\kappa r \sin(\vartheta - \frac{\pi}{6})\} + \cos\{2\kappa r \sin(\vartheta - \frac{\pi}{2})\}}{3}.$$

The polar coordinate form shows the invariance of θ under a hexagonal rotation, that is, invariance to rotation by $\pi/3$; thus

$$\theta(r, \vartheta) = \theta\left(r, \vartheta + \frac{\pi}{3}\right) = \mathcal{H}\theta(r, \vartheta) = \theta(r, \vartheta),$$

where \mathcal{H} is the hexagonal rotation operator.

As an illustrative example, assume that the uniform steady state is unstable to modes for the case $k_c^2 = 4\pi^2$ on the domain $(2\sqrt{3}, 2)$. The corresponding mode pairs are $(6, 2)$ and $(0, 4)$ so that the two wavevectors have the required form (3.9), where $\kappa = \pi$. The resulting pattern is shown in Figure 2. Note that hexagonal solutions not only satisfy zero-flux conditions on the boundaries of a rectangular domain, but do so also on all the hexagonal symmetry boundaries.

Naturally, where we have a triple or higher multiple eigenvalue, a much richer and more complex range of linear patterns is possible.

We have only considered linear solutions in this section. It is, however, important to realize that linear analysis gives only a rough indication as to the patterns we should expect from nonlinear systems. To fully investigate our nonlinear tissue interaction problem (2.5), a weakly nonlinear analysis as well as numerical simulations are necessary.

4. Nonlinear bifurcation analysis. We consider, as mentioned above, the two-dimensional system on the rectangular domain $\mathbf{B} = (L_x, L_y)$ and assume the zero-flux boundary conditions as given in (2.6). We further choose the magnitude of the dimensions L_x and L_y so that stability is lost at an isolated multiple eigenvalue k_c^2 . We perform a perturbation analysis in the neighborhood of this eigenvalue by setting

$$(4.1) \quad \alpha = \alpha_c + \alpha_1\epsilon + \alpha_2\epsilon^2 + \alpha_3\epsilon^3 + \cdots, \quad \text{where } 0 < \epsilon \ll 1,$$

and also

$$(4.2) \quad t = T_1/\epsilon + T_2/\epsilon^2 + T_3/\epsilon^3 + \dots,$$

thus introducing the multiple time scales

$$T_1 = \epsilon t, \quad T_2 = \epsilon^2 t, \quad T_3 = \epsilon^3 t,$$

and so on (refer to Matkowsky (1970)).

We assume a power series expansion for θ and n of the form

$$(4.3a) \quad \theta(\mathbf{x}, \epsilon, T_1, \dots) = \epsilon \theta_1(\mathbf{x}, T_1, \dots) + \epsilon^2 \theta_2(\mathbf{x}, T_1, \dots) + \dots,$$

$$(4.3b) \quad n(\mathbf{x}, \epsilon, T_1, \dots) = 1 + \epsilon n_1(\mathbf{x}, T_1, \dots) + \epsilon^2 n_2(\mathbf{x}, T_1, \dots) + \dots,$$

where the variables θ and n are considered as functions of \mathbf{x} , ϵ , and T_i , $i = 1, 2, 3, \dots$

For algebraic simplicity we initially set

$$\tilde{n}(\mathbf{x}, \epsilon, T_1, \dots) = 1 - n(\mathbf{x}, \epsilon, T_1, \dots)$$

and substitute this into the interaction term of equation (2.5a). The interaction term is then expanded in its Taylor series about $\tilde{n} = 0$,

$$(4.4) \quad \frac{\tau(1 + \tilde{n})^2}{1 + c(1 + \tilde{n})^2} = p_0 + p_1 \tilde{n} + p_2 \tilde{n}^2 + p_3 \tilde{n}^3 + O(\epsilon^4),$$

where the expressions for p_i are given in Appendix A.

As in the one-dimensional case, our system can be written in the form

$$(4.5) \quad \mathcal{L} \begin{pmatrix} \theta \\ \tilde{n} \end{pmatrix} = \mathbf{G} + \mathbf{E},$$

where \mathcal{L} is the linear operator, \mathbf{G} is the function arising from the nonlinear terms, and \mathbf{E} is the function arising from the dependence of α on ϵ and the time derivatives. We have

$$\mathcal{L} \equiv \begin{pmatrix} -\beta \nabla^4 + \nabla^2 - \rho & p_1 \nabla^2 \\ \alpha_c \nabla^2 & D \nabla^2 \end{pmatrix}.$$

As before we denote the components of a two-dimensional vector by the superscripts (1) and (2), so

$$G^{(1)} = -\nabla^2(p_2 \tilde{n}^2 + p_3 \tilde{n}^3) + O(\epsilon^4),$$

$$G^{(2)} = -\alpha_c \nabla \cdot (\tilde{n} \nabla \theta) + O(\epsilon^4),$$

and

$$E^{(1)} = 0,$$

$$E^{(2)} = -\nabla \cdot \{(\tilde{n} + 1) \nabla(\alpha_1 + \epsilon \alpha_2) \epsilon \theta\} + \epsilon \frac{\partial \tilde{n}}{\partial T_1} + \epsilon^2 \frac{\partial \tilde{n}}{\partial T_2} + O(\epsilon^4).$$

The matrix $\mathbf{L}_{(\phi, \psi)}$, arising from applying the operator \mathcal{L} on terms of the form $e^{i(\phi, \psi) \cdot \mathbf{x}}$, is defined as

$$\mathbf{L}_{(\phi, \psi)} = \begin{pmatrix} -\beta(\phi^2 + \psi^2)^2 - (\phi^2 + \psi^2) - \rho & -p_1(\phi^2 + \psi^2) \\ -\alpha_c(\phi^2 + \psi^2) & -D(\phi^2 + \psi^2) \end{pmatrix}.$$

By substituting the series expansions (4.3) into (4.5) and equating coefficients of powers of ϵ , the system of nonlinear equations is reduced to a hierarchy of linear equations.

Equating coefficients of $O(\epsilon)$ gives

$$\mathcal{L} \begin{pmatrix} \theta_1 \\ n_1 \end{pmatrix} = \mathbf{0}.$$

We assume that k_c^2 is the only unstable eigenvalue with corresponding modes growing on the long time scale. Solving the $O(\epsilon)$ equation gives

$$(4.6) \quad \begin{pmatrix} \theta_1 \\ n_1 \end{pmatrix} = \sum_{i=1}^{\Delta} \begin{pmatrix} 1 \\ M_i \end{pmatrix} A_i(T_1, T_2) \cos \phi_i x \cos \psi_i y,$$

where Δ is the multiplicity of the eigenvalue and the functions $A_i(T_1, T_2)$ are the slow time dependent amplitudes. As before, for notational convenience, we only consider the A_i as functions of T_1 and T_2 . Since $\mathbf{k}_c = (\phi_i, \psi_i)^T$ the unstable eigenvalue satisfies

$$k_c^2 = \phi_i^2 + \psi_i^2,$$

where

$$\phi_i = \frac{\tilde{\phi}_i \pi}{L_x}, \quad \psi_i = \frac{\tilde{\psi}_i \pi}{L_y}, \quad i = 1, 2, \dots, \Delta,$$

and $\tilde{\phi}_i, \tilde{\psi}_i$ can only take on nonnegative integer values. Since

$$\mathbf{L}_{(\phi_i, \psi_i)} \begin{pmatrix} 1 \\ M_i \end{pmatrix} = \mathbf{0},$$

we find that

$$M = M_i = -\frac{\alpha_c}{D}.$$

At $O(\epsilon^2)$,

$$\mathcal{L} \begin{pmatrix} \theta_2 \\ n_2 \end{pmatrix} = \mathbf{S},$$

where

$$(4.7a) \quad S^{(1)} = -p_2 \nabla n_1^2,$$

$$(4.7b) \quad S^{(2)} = -\alpha_c \nabla \cdot (n_1 \nabla \theta_1) - \alpha_1 \nabla^2 \theta_1 + \frac{\partial n_1}{\partial T_1}.$$

By substituting θ_1 and n_1 into the above equations, we can find the expression for \mathbf{S} .

Terms of the form $\cos \phi_i x \cos \psi_i y$ appear in the right-hand side of this equation if integers i, j , and k exist, where $1 \leq i, j, k \leq \Delta$, and $i \neq j$, so that

$$\phi_i + \phi_j = \phi_k \quad \text{and} \quad \psi_i - \psi_j = \psi_k$$

or

$$(4.8) \quad \phi_i - \phi_j = \phi_k \quad \text{and} \quad \psi_i + \psi_j = \psi_k.$$

Since these terms are solutions of the homogeneous problem

$$\mathcal{L} \begin{pmatrix} \theta_2 \\ n_2 \end{pmatrix} = \mathbf{0},$$

secular terms arise in the particular solution for $(\theta_2, n_2)^T$. If these secular terms do appear, we suppress them by making use of the Fredholm alternative (see, for example, Keener (1988)). The full details are discussed below.

Even if conditions (4.8) are not satisfied, secular terms still appear in the $O(\epsilon^2)$ solution because of the last two terms in the expression for \mathbf{S} ; see (4.7). We suppress these secular terms by setting $\alpha_1 = 0$ and $T_1 = 0$ in our power series expansions (4.1) and (4.2) so that the amplitudes A_i are now dependent only on T_2 .

The solution of (4.7) consists of a complimentary function and a particular integral and so we write

$$(4.9) \quad \begin{pmatrix} \theta_2 \\ n_2 \end{pmatrix} = \begin{pmatrix} \theta_2^h \\ n_2^h \end{pmatrix} + \begin{pmatrix} \theta_2^p \\ n_2^p \end{pmatrix},$$

where the complimentary solution

$$\begin{pmatrix} \theta_2^h \\ n_2^h \end{pmatrix} = \sum_{i=1}^{\Delta} \mathbf{C}_i \cos \phi_i x \cos \psi_i y,$$

with \mathbf{C}_i a vector function of T_i , $i = 2, 3, \dots$
 At $O(\epsilon^3)$,

$$(4.10) \quad \mathcal{L} \begin{pmatrix} \theta_3 \\ n_3 \end{pmatrix} = \mathbf{R},$$

where

$$R^{(1)} = -\nabla^2(2p_2 n_1 n_2 + p_3 n_1^3),$$

$$R^{(2)} = -\nabla \alpha_c \cdot (n_1 \nabla \theta_2) - \nabla \alpha_c \cdot (n_2 \nabla \theta_1) - \alpha_2 \nabla^2 \theta_1 + \frac{\partial n_1}{\partial T_2}.$$

The expression for \mathbf{R} , after substituting the expressions for n_1 , n_2 , θ_1 , and θ_2 , can be written in the following form

$$(4.11) \quad \begin{aligned} \mathbf{R} = & \mathbf{R}_0(\cos \phi_i x, \cos \psi_i y) + \mathbf{R}_1(\cos(\phi_i \pm 2\phi_j)x, \cos \psi_i y) \\ & + \mathbf{R}_2(\cos \phi_i x, \cos(\psi_i \pm 2\psi_j)y) + \mathbf{R}_3(\cos 3\phi_i x, \cos \psi_i y) \\ & + \mathbf{R}_4(\cos \phi_i x, \cos 3\psi_i y) + \mathbf{R}_5. \end{aligned}$$

The expression \mathbf{R}_5 consists of terms of the form

$$\begin{aligned} & \cos 3\phi_i x \cos 3\psi_i y, \quad \cos(\phi_i \pm 2\phi_j)x \cos(\psi_i \pm 2\psi_j)y, \\ & \cos(\phi_i \pm \phi_j \pm \phi_l)x \cos(\phi_i \pm \phi_j \pm \phi_l)y, \end{aligned}$$

where $i \neq j \neq l$, $1 \leq i, j, l \leq \Delta$, and each \pm -operator should be considered as being independent of preceding \pm -operators. As is evident from the text, the actual expression for \mathbf{R}_5 is not required in the analysis.

The vector \mathbf{R} contains terms of the form $\cos \phi_i x \cos \psi_i y$, which are solutions of the homogeneous problem

$$(4.12) \quad \mathcal{L} \begin{pmatrix} \theta_3 \\ n_3 \end{pmatrix} = \mathbf{0},$$

so that they give rise to secular terms in the solution for $(\theta_3, n_3)^T$. Again we use the Fredholm alternative to suppress these secular terms as we shall show below. This leads to the typical Landau-type amplitude equations. To determine the amplitude equations when the multiplicity of the eigenvalue is higher than two involves highly complex algebraic manipulation. We therefore restrict our analysis to the simpler cases where $\Delta = 1$ and $\Delta = 2$. There are three main cases to consider.

$\Delta = 1$. If $\Delta = 1$, then $\phi_1 = \psi_1 = \phi$ and secular terms appear in the $O(\epsilon^3)$ solution. To suppress these secular terms we use the Fredholm alternative. A solution $\mathbf{w} = (\theta_3, n_3)$ exists for (4.10) if and only if the Fredholm alternative is satisfied, that is, the inner product

$$\langle \mathbf{w}^*, \mathbf{R} \rangle = 0,$$

where \mathbf{w}^* is the bounded solution of the adjoint problem to (4.12) and the inner product is defined as

$$\langle \mathbf{v}, \mathbf{w} \rangle = \lim_{T_2 \rightarrow \infty} \frac{1}{T_2 L_x L_y} \int_0^{T_2} \int_0^{L_x} \int_0^{L_y} \left(v^{(1)} \bar{w}^{(1)} + v^{(2)} \bar{w}^{(2)} \right) dy dx dT,$$

where the bar denotes the complex conjugate.

It is simple to show that the adjoint operator to \mathcal{L} is \mathcal{L}^T . The solution of the adjoint homogeneous problem is therefore

$$(4.13) \quad \mathbf{w}^* = \begin{pmatrix} 1 \\ M^* \end{pmatrix} A^* \cos \phi x \cos \psi y,$$

where A^* is real and

$$M^* = -\frac{p_1}{D}.$$

We find the Landau equation

$$(4.14) \quad \frac{dA_1(T_2)}{dT_2} = \alpha_2 \Gamma A_1(T_2) + \Omega A_1^3(T_2),$$

where the expressions for Γ and Ω are given in Appendix B.

Here, A_1 is the amplitude to $O(\epsilon)$ of the epithelial dilation solution θ . Note that Γ is the initial exponential growth rate of the solution and that $\Gamma > 0$, since $M < 0$. Since the signs of Ω and α_2 can vary, we have four different types of behavior when $T_2 \rightarrow \infty$; see, for example Cruywagen and Murray (1992). It is easy to show, however, that the solution of (4.14) only evolves to a nonhomogeneous bounded steady state if we are in the parameter space where $\Omega < 0$ and have a supercritical bifurcation; thus $\alpha_2 > 0$.

We can assume, without loss of generality, that $\alpha_2 = 1$. The amplitude of θ is then $(-\Gamma/\Omega)^{\frac{1}{2}}$, while that of n is $M(-\Omega/\Gamma)^{\frac{1}{2}}$. With zero-flux boundary conditions the steady-state solution that emerges is

$$(4.15) \quad \begin{pmatrix} \theta \\ n \end{pmatrix} = \begin{pmatrix} 0 \\ 1 \end{pmatrix} + \epsilon \left(-\frac{\Omega}{\Gamma} \right)^{\frac{1}{2}} \begin{pmatrix} 1 \\ M \end{pmatrix} \cos \phi x \cos \phi y + O(\epsilon^2) \text{ as } T_2 \rightarrow \infty.$$

We examine some specific numerical examples in the next section to test the accuracy of this analytical solution.

$\Delta = 2$ and secular terms appear at $O(\epsilon^2)$. From (4.8) we know that for $\Delta = 2$, secular terms already appear in the $O(\epsilon^2)$ solution (4.9) when, for $i, j = 1, 2$ and $i \neq j$,

$$\phi_i + \phi_j = \phi_j \text{ and } \psi_i - \psi_j = \psi_j$$

or

$$(4.16) \quad \phi_i - \phi_j = \phi_j \text{ and } \psi_i + \psi_j = \psi_j.$$

This is true if, for example,

$$(4.17) \quad \phi_1 = \phi, \quad \psi_1 = \sqrt{3}\phi, \quad \phi_2 = 2\phi, \quad \psi_2 = 0$$

for any ϕ . Since our system of equations (2.5) is translation invariant in x and y and the analysis is not affected by a translation of wavevectors, it is sufficient to consider only this case. As we have seen in the linear analysis of the previous section, see (3.8) and (3.9), hexagonal patterns fall within this class of solutions.

Here the inner product is defined as

$$(4.18) \quad \langle \mathbf{v}, \mathbf{w} \rangle = \lim_{T_1 \rightarrow \infty} \frac{1}{T_1 L_x L_y} \int_0^{T_1} \int_0^{L_x} \int_0^{L_y} (v^{(1)} \bar{w}^{(1)} + v^{(2)} \bar{w}^{(2)}) dy dx dT.$$

It is easy to show that the solutions of the adjoint problem to

$$\mathcal{L} \begin{pmatrix} \theta_2 \\ n_2 \end{pmatrix} = \mathbf{0}$$

are

$$\mathbf{w}_1^* = A_1^* \begin{pmatrix} 1 \\ M^* \end{pmatrix} \cos \phi x \cos \sqrt{3}\phi y, \quad \mathbf{w}_2^* = A_2^* \begin{pmatrix} 1 \\ M^* \end{pmatrix} \cos 2\phi x,$$

where A_1^* and A_2^* are arbitrary real constants and, as before, $M^* = -p_1/D$.

Now calculating $\langle \mathbf{w}_1^*, \mathbf{S} \rangle = 0$ and similarly for \mathbf{w}_2^* we find the two amplitude equations

$$(4.19a) \quad \frac{dA_1}{dT_1} = \alpha_1 \Gamma A_1 + \Omega A_1 A_2,$$

$$(4.19b) \quad \frac{dA_2}{dT_1} = \alpha_1 \Gamma A_2 + \frac{1}{4} \Omega A_1^2,$$

where Γ and Ω are given in Appendix B. From the linear analysis we know that the homogeneous steady state loses stability at a supercritical bifurcation; thus $\alpha_1 > 0$.

The time-independent solutions for system (4.19) are

$$A_1^{(s_0)} = 0, \quad A_2^{(s_0)} = 0,$$

and

$$A_1^{(s_1)} = \pm \frac{4\alpha_1 p_1}{M(2MDp_2 - \alpha_c p_1)}, \quad A_2^{(s_1)} = \frac{2\alpha_1 p_1}{M(2MDp_2 - \alpha_c p_1)},$$

so $A_1^{(s_1)} = \pm 2A_2^{(s_1)}$. The different solutions $A_1^{(s_1)} = 2A_2^{(s_1)}$ and $A_1^{(s_1)} = -2A_2^{(s_1)}$ merely give patterns of different phases. Without loss of generality we only consider the case $A_1^{(s_1)} = 2A_2^{(s_1)}$.

The stability of each solution $(A_1^{(s_i)}, A_2^{(s_i)})^T$, $i = 0, 1$, is determined from a linear stability analysis of equations (4.19) about the steady state. Thus, in the usual way, we substitute

$$A_1 = A_1^{(s_i)} + \tilde{A}_1, \quad A_2 = A_2^{(s_i)} + \tilde{A}_2, \quad i = 0, 1,$$

into (4.19), where $|\tilde{A}_1| \ll 1$ and $|\tilde{A}_2| \ll 1$. Now the stability of the perturbations about the solutions $(A_1^{(s_i)}, A_2^{(s_i)})^T$ is determined by the eigenvalues of the matrix \mathcal{M} where

$$(4.20) \quad \mathcal{M} = \begin{pmatrix} m_{1,1} & m_{1,2} \\ m_{2,1} & m_{2,2} \end{pmatrix}.$$

For the expressions of the components of \mathcal{M} refer to Appendix C. The eigenvalues of this system are

$$\lambda = \frac{1}{2}m_{2,2} \pm \frac{1}{2}\sqrt{m_{2,2}^2 + 4m_{1,2}m_{2,1}},$$

and since $m_{2,2} > 0$ and $m_{1,2}m_{2,1} > 0$, they are always positive. Thus no stable steady-state pattern is possible for this specific mode combination.

Since hexagonal patterns fall within the class of patterns considered here, the nonlinear analysis therefore predicts that our small strain quasi-steady-state tissue interaction system does *not* exhibit steady-state hexagonal patterned solutions arising as primary bifurcations from the uniform steady state (but see section 5, Example 5.6).

$\Delta = 2$ and secular terms appear at $O(\epsilon^3)$. For $\Delta = 2$ secular terms appear in the $O(\epsilon^3)$ solution when the unstable eigenvalue is such that the two corresponding allowable wavevectors do not satisfy conditions (4.16). Suppressing secular terms as in the previous two cases leads to the system of Landau equations

$$(4.21a) \quad \frac{dA_1}{dT_2} = \alpha_2\Gamma A_1 + \Omega_1 A_1^3 + \Upsilon_1 A_1 A_2^2,$$

$$(4.21b) \quad \frac{dA_2}{dT_2} = \alpha_2\Gamma A_2 + \Omega_2 A_2^3 + \Upsilon_2 A_1^2 A_2,$$

where

$$\Gamma = -\frac{\phi_1^2 + \psi_1^2}{M} > 0.$$

The expressions for Ω_1 , Ω_2 , Υ_1 , and Υ_2 depend on the specific wavevectors involved as we shall see below.

The four time-independent solutions of this system and the conditions for their existence are

$$(4.22) \quad \begin{aligned} A_1^{(s_0)} &= 0, & A_2^{(s_0)} &= 0, \\ (A_1^{(s_1)})^2 &= -\frac{\alpha_2\Gamma}{\Omega_1} > 0, & A_2^{(s_1)} &= 0, \\ A_1^{(s_2)} &= 0, & (A_2^{(s_2)})^2 &= -\frac{\alpha_2\Gamma}{\Omega_2} > 0, \\ (A_1^{(s_3)})^2 &= \frac{\alpha_2\Gamma(\Upsilon_1 - \Omega_2)}{\Omega_1\Omega_2 - \Upsilon_1\Upsilon_2} > 0, & (A_2^{(s_3)})^2 &= \frac{\alpha_2\Gamma(\Upsilon_2 - \Omega_1)}{\Omega_1\Omega_2 - \Upsilon_1\Upsilon_2} > 0. \end{aligned}$$

Linearizing (4.21) about the steady states we find, as before, that the linear stability of the steady states is determined by the eigenvalues of the matrix \mathcal{M} (see (4.20)), which are

$$(4.23) \quad \lambda = \frac{1}{2}(m_{1,1} + m_{2,2}) \pm \frac{1}{2}\sqrt{(m_{1,1} - m_{2,2})^2 + 4m_{1,2}m_{2,1}}.$$

The expressions for the components of \mathcal{M} , $m_{i,j}$ are given in Appendix C. The signs of the eigenvalues and thus the stability properties of the steady states are dependent on the parameter values.

The linear analysis predicted that pattern formation would only be possible for (2.5) if we have a supercritical bifurcation; that is, $\alpha_2 > 0$. Without loss of generality we therefore assume that $\alpha_2 = 1$.

We have three nonhomogeneous steady-state solutions for large time, two single mode steady states and a mixed mode steady state. They are given by

$$(4.24a) \quad \begin{pmatrix} \theta \\ n \end{pmatrix} = \begin{pmatrix} 0 \\ 1 \end{pmatrix} + \epsilon A_1^{(s_1)} \begin{pmatrix} 1 \\ M \end{pmatrix} \cos \phi_1 x \cos \psi_1 y + O(\epsilon^2),$$

$$(4.24b) \quad \begin{pmatrix} \theta \\ n \end{pmatrix} = \begin{pmatrix} 0 \\ 1 \end{pmatrix} + \epsilon A_2^{(s_2)} \begin{pmatrix} 1 \\ M \end{pmatrix} \cos \phi_2 x \cos \psi_2 y + O(\epsilon^2),$$

$$(4.24c) \quad \begin{pmatrix} \theta \\ n \end{pmatrix} = \begin{pmatrix} 0 \\ 1 \end{pmatrix} + \epsilon A_1^{(s_3)} \begin{pmatrix} 1 \\ M \end{pmatrix} \cos \phi_1 x \cos \psi_1 y + \epsilon A_2^{(s_3)} \begin{pmatrix} 1 \\ M \end{pmatrix} \cos \phi_2 x \cos \psi_2 y + O(\epsilon^2),$$

where the different $A_1^{(s_i)}$ and $A_2^{(s_i)}$ are the steady states (4.24) of the Landau equations (4.21), respectively.

We next discuss the forms which the expressions $\Omega_1, \Omega_2, \Upsilon_1$, and Υ_2 take. There are three cases to consider.

Case 1. If $\phi_i \neq 0$ and $\psi_i \neq 0, i = 1, 2$, then terms of the form $\cos \phi_i x \cos \psi_i y$ appear only in the expression for \mathbf{R}_0 in equation (4.11). The values of Ω_1, Ω_2 , and $\Upsilon = \Upsilon_1 = \Upsilon_2$ obtained after using the Fredholm alternative are given in Appendix D.

Case 2. If one and only one of ϕ_i or $\psi_i, i = 1, 2$ is equal to zero, then terms of the form $\cos \phi_i x \cos \psi_i y$ not only appear in the expression for \mathbf{R}_0 but also in \mathbf{R}_1 or \mathbf{R}_2 and \mathbf{R}_3 or \mathbf{R}_4 (see equation (4.11)). As before it is sufficient to consider only one case, say

$$\phi_1 \neq 0, \quad \psi_1 \neq 0, \quad \phi_2 = 0, \quad \psi_2 \neq 0,$$

where $\phi_1^2 + \psi_1^2 = \psi_2^2$.

For this particular set of wavevectors, terms of the form $\cos \phi_i x \cos \psi_i y$ appear in $\mathbf{R}_0, \mathbf{R}_1$, and \mathbf{R}_3 . Suppressing the secular terms results in the same expressions for Ω_1 and Υ_2 as in Case 1 above. Expressions for Ω_2 and Υ_2 are given in Appendix D.

Case 3. If one and only one of $\phi_1 = \psi_2 = 0$ or $\phi_2 = \psi_1 = 0$ is true, then terms of the form $\cos \phi_i x \cos \psi_i y$ appear in the expression for $\mathbf{R}_0, \mathbf{R}_1$ or \mathbf{R}_2 , and \mathbf{R}_3 or \mathbf{R}_4 (see equation (4.11)). Again it is sufficient to consider only one combination of wavevectors, say

$$\phi_1 = \phi, \quad \psi_1 = 0, \quad \phi_2 = 0, \quad \psi_2 = \phi.$$

The values of Ω_1, Ω_2 , and $\Upsilon = \Upsilon_1 = \Upsilon_2$ obtained after using the Fredholm alternative are given in Appendix D.

This weakly nonlinear analysis gives a good indication of what type of patterns to expect as well as parameter ranges for which various steady-state patterns would exist. Numerical simulations for specific examples are considered in the next section to verify our calculations and to illustrate some of the patterns exhibited by the model.

5. Numerical simulations. In this section we use numerical methods to solve the reduced small strain quasi-steady-state system (2.5) on rectangular domains. We select parameters so that we are in the vicinity of a primary bifurcation point from the uniform steady state. The numerical results can then be compared with those predicted by the bifurcation analysis of the previous section.

An implicit finite difference numerical scheme is used to solve the nonlinear equations (2.5). For examples where the small parameter $\epsilon = 0.1$, the computation took on average about 15 to 20 hours CPU time to reach a steady-state solution on a DEC5500 Risc Ultrix computer. For smaller values of ϵ , for example, $\epsilon = 0.01$, the growth rate of the patterns are even slower so that it becomes impractical to solve the model equations in real time.

In the first example we solve the system for parameter values such that the uniform steady state is linearly unstable to only one mode. In all the other examples, the uniform steady state is linearly unstable to two modes. As initial conditions we used random perturbations with minimum and maximum values ± 0.001 , about the homogeneous steady state $\theta = 0$, $n = 1$, to simulate the natural inhomogeneties present in skin tissue.

To ensure that the numerical method employed is stable and convergent we solved the equations using different mesh sizes in both time and space. Because of computer time constraints we never used more than a 1000 mesh points for discretizing the rectangle \mathbf{B} .

Example 5.1. We consider system (2.5) and isolate the eigenvalue $k_c^2 = 4\pi^2$. For isolating an eigenvalue, say k_c^2 , the following two equations must be satisfied:

$$(5.1a) \quad \beta k_c^4 - \rho = 0,$$

$$(5.1b) \quad (\alpha_c P_2 - D)k_c^2 - 2\rho D = 0.$$

For linear instability, the value of the bifurcation parameter, α in this case, must be increased marginally beyond the critical value α_c .

One set of parameter values that satisfies the above equations when $k_c^2 = 4\pi^2$ is

$$\beta = 0.0126651, \quad \rho = 19.7369, \quad \tau = 4.0, \quad c = 1.0, \quad D = 2.0, \quad \alpha_c = 2.0.$$

On the square domain $(\sqrt{2}, \sqrt{2})$, these parameter values result in the (2, 2) mode being isolated. The analytical prediction for the steady state pattern, as obtained in the nonlinear analysis of the previous section, is therefore given in (4.15). We computed the expressions for Ω and Γ (see equation (4.14)) for the above parameter set. With $\epsilon = 0.1$ the predicted solution for large time is

$$\theta(x, y, t) \approx 0.16 \cos\left(\frac{2\pi x}{\sqrt{2}}\right) \cos\left(\frac{2\pi y}{\sqrt{2}}\right),$$

$$n(x, y, t) \approx 1 - 0.16 \cos\left(\frac{2\pi x}{\sqrt{2}}\right) \cos\left(\frac{2\pi y}{\sqrt{2}}\right).$$

This is in excellent agreement with the numerically computed solutions for θ and n which reach maximum and minimum amplitudes for large time of 0.16 and -0.16 , respectively.

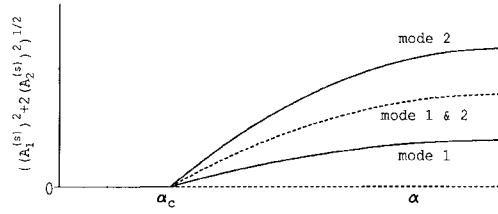


FIG. 3. The qualitative bifurcation diagram for the steady-state solutions associated with various mode pairs of system (4.19) when the parameter values are as in Example 5.2. The two mode pairs are (2, 3) and (3, 2). Solid lines indicate stable steady states, while broken lines indicate unstable steady states.

Example 5.2. In this example the model parameters are selected so as to isolate the eigenvalue $k_c^2 = 6.5\pi^2$. By using equations (5.1) we find that a possible parameter set is

$$\beta = 0.00779393, \quad \rho = 32.0762, \quad \tau = 4.0, \quad c = 1.0, \quad D = 2.0, \quad \alpha_c = 2.0.$$

As in the first example, we consider the problem on the domain $(\sqrt{2}, \sqrt{2})$; however, in this case, the uniform steady state is linearly unstable to two modes, namely (2, 3) and (3, 2).

We can now use expressions (4.22) for determining the steady states and (4.23) for determining their stability. Note that the values of Ω_i and Υ_i are as in Case 1. There are three nonhomogeneous steady states—two single mode steady states which are stable and a mixed mode steady state which is unstable. We can now construct the bifurcation diagram as predicted by the nonlinear analysis. So as to separate the two single mode steady states on the bifurcation diagram when they have the same value, we plot the bifurcation parameter α_c against the value $\sqrt{A_1^{(s_i)} + 2A_1^{(s_i)}}$ (see Figure 3).

The amplitudes of the steady-state solutions were computed from (4.22) and the predicted solutions (see (4.24)) are

$$\theta(x, y, t) \approx 0.16 \cos\left(\frac{2\pi x}{\sqrt{2}}\right) \cos\left(\frac{3\pi y}{\sqrt{2}}\right),$$

$$n(x, y, t) \approx 1.0 - 0.16 \cos\left(\frac{2\pi x}{\sqrt{2}}\right) \cos\left(\frac{3\pi y}{\sqrt{2}}\right)$$

or

$$\theta(x, y, t) \approx 0.16 \cos\left(\frac{3\pi x}{\sqrt{2}}\right) \cos\left(\frac{2\pi y}{\sqrt{2}}\right),$$

$$n(x, y, t) \approx 1.0 - 0.16 \cos\left(\frac{3\pi x}{\sqrt{2}}\right) \cos\left(\frac{2\pi y}{\sqrt{2}}\right).$$

Since we are dealing with a square domain and the problem is invariant under a change of x and y , the above two solutions are equivalent. Our numerical solutions have maximum and minimum values of 0.17 and -0.17 , respectively, which compare very well with our analytical predictions as shown in Figure 4.

Example 5.3. By selecting the parameter set

$$\beta = 0.005960, \quad \rho = 41.9458, \quad \tau = 4.2025, \quad c = 1.05, \quad D = 2.0, \quad \alpha = 2.0,$$

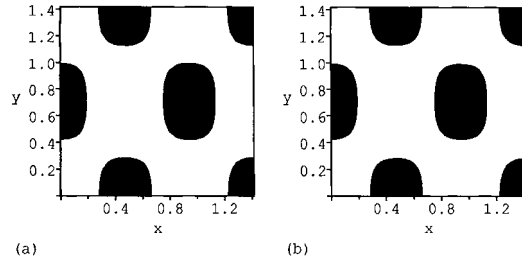


FIG. 4. The computed dilation solution θ for parameter values as in Example 5.2 is shown in the contour graph (a), while the predicted solution is shown in (b). Regions where $\theta \geq 0.05$ are shaded in both graphs.

we isolate the unstable eigenvalue $k_c^2 = 8.5\pi^2$. On the square domain $(\sqrt{2}, \sqrt{2})$ the uniform steady state is linearly unstable to the modes $(1, 4)$ and $(4, 1)$. The bifurcation diagram, calculated from our nonlinear analysis, is similar to that in Figure 3. Here, however, the mixed mode solution is stable, while the two single mode solutions are unstable. So the expected solution is

$$\theta(x, y, t) \approx 0.14 \cos\left(\frac{\pi x}{\sqrt{2}}\right) \cos\left(\frac{4\pi y}{\sqrt{2}}\right) + 0.14 \cos\left(\frac{4\pi x}{\sqrt{2}}\right) \cos\left(\frac{\pi y}{\sqrt{2}}\right),$$

$$n(x, y, t) \approx 1.0 - 0.14 \cos\left(\frac{\pi x}{\sqrt{2}}\right) \cos\left(\frac{4\pi y}{\sqrt{2}}\right) + 0.14 \cos\left(\frac{4\pi x}{\sqrt{2}}\right) \cos\left(\frac{\pi y}{\sqrt{2}}\right).$$

The numerical simulations of the nonlinear system do indeed evolve to a mixed mode solution, as seen in Figure 5. Although the peaks in our numerical solution are not as high as those in our predicted solution, the troughs are almost of equal depth, and the two solutions share similar characteristics. Hence the solutions are qualitatively similar.

Example 5.4. Here we select the parameters

$$\beta = 0.00405285, \quad \rho = 61.6850, \quad \tau = 4.5, \quad c = 1.12132, \quad D = 2.0, \quad \alpha = 2.0,$$

to isolate the unstable eigenvalue $k_c^2 = 12.5\pi^2$. If we consider the system of equations on the rectangular domain $(\sqrt{2}, \sqrt{2}/2)$, the uniform steady state is linearly unstable to the modes $(5, 0)$ and $(3, 2)$. Our bifurcation diagram allows for only the two single mode steady states—one is stable and the other unstable (see Figure 6).

The expressions for Ω_i and Υ_i , $i = 1, 2$, are as in Case 2. The predicted steady-state solution is

$$\theta(x, y, t) \approx 0.23 \cos\left(\frac{3}{\sqrt{2}}\pi x\right) \cos\left(\frac{4\pi y}{\sqrt{2}}\right),$$

$$n(x, y, t) \approx 1.0 - 0.23 \cos\left(\frac{3}{\sqrt{2}}\pi x\right) \cos\left(\frac{4\pi y}{\sqrt{2}}\right).$$

For both random initial conditions and stripe-like initial conditions resembling the mode $(5, 0)$, we found a steady-state solution resembling the predicted mode. The troughs of the computed pattern have minimum values -0.23 , while the peaks have a maximum value of 0.28 . The error is therefore $O(\epsilon^2)$ as expected.

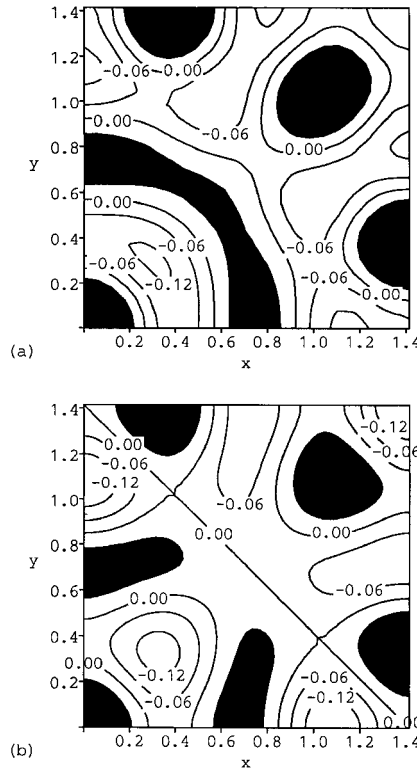


FIG. 5. The numerically computed contour graph of the dilation θ when the parameter values are as in Example 5.3. The solution predicted by the nonlinear analysis is shown in (b). Note that we have a mixed mode steady state here. Regions where $\theta > 0.07$ are shaded in both graphs.

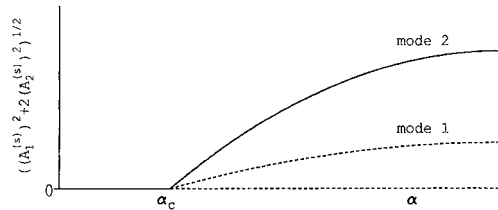


FIG. 6. The qualitative bifurcation diagram for the steady-state solutions of system (4.19) when the parameter values are as in Example 5.4. The steady state associated with the first mode pair, $(5, 0)$, is unstable and that associated with the second, $(3, 2)$, is stable.

Example 5.5. In this example we isolate the unstable eigenvalue satisfying $k_c^2 = 9\pi^2$. To do this we choose the parameters

$$\beta = 0.00562895, \quad \rho = 44.4132, \quad \tau = 4.8, \quad c = 1.19089, \quad D = 2.0, \quad \alpha = 2.0.$$

We consider the problem on the square domain $(1, 1)$ so that the uniform steady state is linearly unstable to the modes $(2, 0)$ and $(0, 2)$. The bifurcation diagram is similar to that in the previous example (see Figure 6) except for the fact that both the nonhomogeneous steady states are now stable. The expressions for Ω_i and Υ_i are

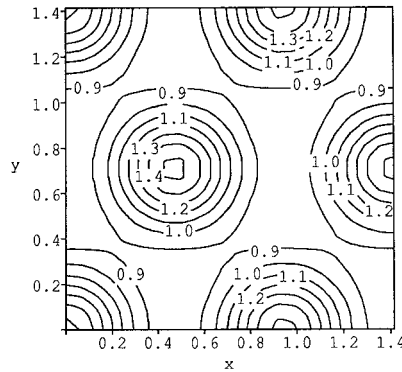


FIG. 7. Contour graph of the numerically computed steady-state solution θ for the parameter set in Example 5.6. A hexagonal-type pattern arises due to a secondary bifurcation.

now as in Case 3. The nonlinear analysis predicts either

$$\begin{aligned}\theta(x, y, t) &\approx 0.30 \cos(3\pi x), \\ n(x, y, t) &\approx 1.0 - 0.30 \cos(3\pi x)\end{aligned}$$

or

$$\begin{aligned}\theta(x, y, t) &\approx 0.30 \cos(3\pi y), \\ n(x, y, t) &\approx 1.0 - 0.30 \cos(3\pi y),\end{aligned}$$

as the steady state solutions. The numerical solutions have amplitudes of ± 0.17 . This is much smaller than predicted, so the nonlinear analysis does not give such accurate results for this case. Qualitatively, however, the solutions are identical.

Example 5.6. We show an example in which the prediction by the weakly nonlinear analysis fails. We isolate the same eigenvalue as in Example 5.2 and use the same parameters except for

$$\tau = 3.0625, \quad c = 0.75.$$

Our bifurcation diagram is similar to that in Example 5.3, so that we expect the mixed mode solution, made up of the mode pairs (2, 3) and (3, 2), to develop. Numerical simulations show, however, that the mixed steady state is only a transient and that a hexagonal-type steady-state pattern eventually develops—each peak is closest to its six nearest neighbors (see Figure 7).

It seems, therefore, that a secondary bifurcation has occurred here. Our nonlinear analysis, however, cannot predict this since it only applies to primary bifurcation points. Therefore, although our weakly nonlinear analysis indicates that hexagonal patterns are not possible, such steady patterns could still evolve due to secondary bifurcations. Another possibility is that an alternative scaling of the equations may give results consistent with our numerical solutions (Wheeler (1985)). Due to the algebraic complexity of the system, we do not pursue this further. The key result is that the numerical simulations show that the model can exhibit stable hexagonal patterns.

In the majority of examples considered, the numerical results agreed well with the perturbation solutions obtained from the multiscale bifurcation analysis. Even better agreement could have been achieved by using smaller values for the perturbation parameter ϵ . Furthermore, the mesh size used in the finite difference approximations was rather crude and a finer mesh would also contribute toward more accurate solutions. However, due to computing time constraints it was impractical to incorporate these features into our simulations.

6. Conclusion. In this paper we have presented a weakly nonlinear analysis to determine the pattern-forming capability of a tissue interaction model for skin organ formation on a rectangular domain. This model hypothesizes that skin organ formation occurs as a result of cell aggregation followed by the differentiation of cells in high density aggregates. This model hypothesis is different from that of reaction diffusion theory, in which it is assumed that cell density remains uniform, but cells differentiate in response to a spatially varying prepatter in some chemical morphogen. There is strong experimental evidence that patterns in the skin arise due to cell aggregation (see, for example, Wessells (1965) and Murray, Deeming, and Ferguson (1990)).

This model differs from others in the literature in that dermal-epidermal tissue interaction is a prerequisite for spatial pattern formation. In this respect, it agrees well with biological observations. We are unaware of other models which reflect this dermal-epidermal interdependence. Most skin pattern formation models give rise to patterns in either layer, completely independent of the other layer.

The bifurcation analysis, although very complex, enabled us to derive parameter spaces in which certain patterns occur. It furthermore provided an indication of the wealth of patterns that the model can exhibit. Due to the large number of model parameters, it would have been an impossible task to identify all the various solutions numerically. However, the analysis we presented, which holds only in the vicinity of primary bifurcation points, is somewhat limited in that the model can also produce other types of patterns. An important class of patterns that cannot arise from a primary bifurcation in this model are hexagonal patterns. Such patterns are considered to be very stable and are common in nature. Recently, a number of studies of hexagonal pattern formation in chemical systems have been carried out (see, for example, Maini, Painter, and Chau (1997)). However, Example 5.6 shows that stable hexagonal patterns can arise in our model as a result of what we conjecture is a secondary bifurcation.

Another limitation of the analysis is that when the uniform steady state is linearly unstable to multiple modes, as in Example 5.2, the domain of attraction of initial conditions for each of the modes cannot be predicted. To determine which solution is preferred for a specific set of initial conditions, the system has to be solved numerically.

In many cases, skin organ patterns are actually laid down sequentially, and it is believed that travelling waves of determination (Zeeman (1974)) often initiate morphogenetic processes. For example, stripe pigment patterns on the alligator develop sequentially. The hexagonal pattern of feather germs observed on dorsal chick skin actually arises as a wave of spatio-temporal pattern sweeps outward from the dorsal midline.

Cruywagen, Maini, and Murray (1992) discuss the modeling of sequential pattern formation and illustrate how the tissue interaction model described here can actually produce patterns sequentially. The more detailed version of the tissue interaction model does in fact possess travelling wave solutions (Cruywagen, Maini, and Murray

(1994a)). The model can also sustain spatial patterns in the wake of a travelling wave (Cruywagen, Maini, and Murray (1994b)).

In this paper, we have shown that a variety of spatial patterns can also occur as stable solutions to the reduced small strain quasi-steady-state system (2.5). The patterns illustrated in Examples 5.1 and 5.6 resemble those of feather germs on chicken skin. The stripe-like pigment patterns seen on alligators are similar to the solution of Example 5.5 (see Murray, Deeming, and Ferguson (1990)). The more complex patterns seen on some vertebrates, especially reptiles, can also be explained by our model via mode interaction as we have shown in Example 5.3.

Appendix A. The expressions for p_i refer to the series expansion in (4.4),

$$\begin{aligned} p_0 &= \frac{\tau}{1+c}, & p_2 &= \frac{\tau(1-3c)}{(1+c)^3}, \\ p_1 &= \frac{2\tau}{(1+c)^2}, & p_3 &= \frac{4\tau c(c-1)}{(1+c)^4}. \end{aligned}$$

Appendix B. The expressions for Γ and Ω as they appear in (4.14) are

$$\begin{aligned} \Gamma &= -\frac{2\phi^2}{M} > 0, \\ \Omega &= -\alpha_c \left(a_1^{(1)} + b_1^{(1)} + d_1^{(1)} - \frac{d_1^{(2)}}{2M} \right) \phi^2 \\ &\quad + \frac{D}{p_1} \left(2p_2 a_1^{(2)} + 2p_2 b_1^{(2)} + p_2 d_1^{(2)} + \frac{9}{8} p_3 M^2 \right) \phi^2. \end{aligned}$$

The expressions for Γ and Ω as they appear in (4.19) are

$$\Gamma = -\frac{4\phi^2}{M} > 0, \quad \Omega = -2\phi^2 \left(\alpha_c - \frac{2Dp_2M}{p_1} \right).$$

Refer to Appendix E for the expressions of \mathbf{a}_i , \mathbf{b}_i , \mathbf{d}_i .

Appendix C. The elements of the matrix \mathcal{M} in (4.20) and their signs are

$$\begin{aligned} m_{1,1} &= 0, & m_{1,2} &= -\frac{8\alpha_1\phi^2}{M} > 0, \\ m_{2,1} &= \frac{4\alpha_1\phi^2}{M} > 0, & m_{2,2} &= -\frac{4\alpha_1\phi^2}{M} > 0 \end{aligned}$$

since $M < 0$ and $\alpha_1 > 0$.

The elements of \mathcal{M} as used in (4.23) are

$$\begin{aligned} m_{1,1} &= \alpha_2\Gamma + 3\Omega_1 \left(A_1^{(s_i)} \right)^2 + \left(\Upsilon_1(A_2^{(s_i)}) \right)^2, \\ m_{1,2} &= 2\Upsilon_1 A_1^{(s_i)} A_2^{(s)}, \\ m_{2,1} &= 2\Upsilon_2 A_1^{(s_i)} A_2^{(s)}, \\ m_{2,2} &= \alpha_2\Gamma + 3\Omega_2 \left(A_2^{(s_i)} \right)^2 + \Upsilon_2 \left(A_1^{(s_i)} \right)^2. \end{aligned}$$

Appendix D. The expressions for Ω_1 , Ω_2 , Υ_1 , and Υ_2 appearing in the Landau equations for the three cases considered when $\Delta = 2$ and secular terms appear at $O(\epsilon^3)$ are given below.

(Refer to Appendix E for the expressions of \mathbf{a}_i , \mathbf{b}_i , \mathbf{d}_i , $\mathbf{a}_{i,j}$, $\mathbf{b}_{i,j}$, $\mathbf{d}_{i,j}$, and $\mathbf{e}_{i,j}$.)

Case 1. We have

$$\begin{aligned} \Omega_1 &= -\alpha_c \left(a_1^{(1)} \phi_1^2 + b_1^{(1)} \psi_1^2 \right) - \frac{1}{2} \alpha_c \left(d_1^{(1)} - \frac{d_1^{(2)}}{2M} \right) (\phi_1^2 + \psi_1^2) \\ &\quad + \frac{D}{p_1} \left(p_2 a_1^{(2)} + p_2 b_1^{(2)} + \frac{1}{2} p_2 d_1^{(2)} + \frac{9}{16} p_3 M^2 \right) (\phi_1^2 + \psi_1^2), \\ \Omega_2 &= -\alpha_c \left(a_2^{(1)} \phi_2^2 + b_2^{(1)} \psi_2^2 \right) - \frac{1}{2} \alpha_c \left(d_2^{(1)} - \frac{d_2^{(2)}}{2M} \right) (\phi_2^2 + \psi_2^2) \\ &\quad + \frac{D}{p_1} \left(p_2 a_2^{(2)} + p_2 b_2^{(2)} + \frac{1}{2} p_2 d_2^{(2)} + \frac{9}{16} M^2 p_3 \right) (\phi_2^2 + \psi_2^2), \end{aligned}$$

and $\Upsilon_1 = \Upsilon_2 = \Upsilon$, where

$$\begin{aligned} \Upsilon &= \frac{D}{4p_1} \left(2p_2 a_{1,2}^{(2)} + 2p_2 b_{1,2}^{(2)} + 2p_2 d_{1,2}^{(2)} + 2p_2 e_{1,2}^{(2)} + 3p_3 M^2 \right) (\phi_1^2 + \psi_1^2) \\ &\quad - \frac{1}{4} \alpha_c \left(a_{1,2}^{(1)} + b_{1,2}^{(1)} + d_{1,2}^{(1)} + e_{1,2}^{(1)} \right) (\phi_1^2 + \psi_1^2) \\ &\quad - \frac{\alpha_c}{4M} \left[\left(a_{1,2}^{(1)} M - a_{1,2}^{(2)} \right) (\phi_1 \phi_2 + \psi_1 \psi_2) \right. \\ &\quad \left. + \left(b_{1,2}^{(1)} M - b_{1,2}^{(2)} \right) (\phi_1 \phi_2 - \psi_1 \psi_2) \right. \\ &\quad \left. + \left(d_{1,2}^{(1)} M - d_{1,2}^{(2)} \right) (-\phi_1 \phi_2 + \psi_1 \psi_2) \right. \\ &\quad \left. + \left(e_{1,2}^{(1)} M - e_{1,2}^{(2)} \right) (-\phi_1 \phi_2 - \psi_1 \psi_2) \right]. \end{aligned}$$

Case 2. The expressions for Ω_1 and Υ_2 are as in Case 1 above:

$$\begin{aligned} \Omega_2 &= -\alpha_c \left(b_2^{(1)} + \frac{1}{2} d_2^{(1)} - \frac{d_2^{(2)}}{4M} \right) \psi_2^2 - \frac{\alpha_c p_1}{2D} \left(d_2^{(1)} M + \frac{1}{2} d_2^{(2)} \right) \psi_2^2 \\ &\quad + \frac{D}{p_1} \left(p_2 b_2^{(2)} + \frac{1}{2} p_2 d_2^{(2)} + \frac{9}{16} p_3 M^2 \right) \psi_2^2 + \frac{M}{2} \left(p_2 d_2^{(2)} + \frac{3}{8} p_3 M^2 \right) \psi_2^2 \end{aligned}$$

and

$$\begin{aligned} \Upsilon_1 &= \Upsilon_2 + \left[2p_2 M a_2^{(2)} + \frac{3}{4} p_3 M^3 + \frac{1}{2} p_2 M \left(a_{1,2}^{(2)} + b_{1,2}^{(2)} + d_{1,2}^{(2)} + e_{1,2}^{(2)} \right) \right] \psi_2^2 \\ &\quad - \frac{p_1 \alpha_c}{D} \left[a_2^{(2)} \psi_2^2 + \frac{1}{4} M \left(a_{1,2}^{(1)} + d_{1,2}^{(1)} \right) (\psi_1^2 + \psi_1 \psi_2) \right. \\ &\quad \left. + \frac{1}{4} M \left(b_{1,2}^{(1)} + e_{1,2}^{(1)} \right) (\psi_1^2 - \psi_1 \psi_2) - \left(a_{1,2}^{(2)} - b_{1,2}^{(2)} + d_{1,2}^{(2)} - e_{1,2}^{(2)} \right) \psi_1 \psi_2 \right]. \end{aligned}$$

Case 3. We have

$$\begin{aligned} \Omega_1 &= -\alpha_c \left(a_1^{(1)} + \frac{1}{2}d_1^{(1)} - \frac{d_1^{(2)}}{4M} \right) \phi^2 - \frac{\alpha_c p_1}{2D} \left(d_1^{(1)} M - \frac{1}{2}d_1^{(2)} \right) \phi^2 \\ &\quad + \frac{1}{2}M \left(p_2 d_1^{(2)} + \frac{3}{8}p_3 M^2 \right) \phi^2 + \frac{D}{p_1} \left(p_2 a_1^{(2)} + \frac{1}{2}p_2 d_1^{(2)} + \frac{9}{16}M^2 p_3 \right) \phi^2, \\ \Omega_2 &= -\alpha_c \left(b_2^{(1)} + \frac{1}{2}d_2^{(1)} - \frac{d_2^{(2)}}{4M} \right) \phi^2 - \frac{\alpha_c p_1}{2D} \left(d_2^{(1)} M - \frac{1}{2}d_2^{(2)} \right) \phi^2 \\ &\quad + \frac{1}{2}M \left(p_2 d_2^{(2)} + \frac{3}{8}p_3 M^2 \right) \phi^2 + \frac{D}{p_1} \left(p_2 b_2^{(2)} + \frac{1}{2}p_2 d_2^{(2)} + \frac{9}{16}M^2 p_3 \right) \phi^2. \end{aligned}$$

Also $\Upsilon_1 = \Upsilon_2 = \Upsilon$ where

$$\begin{aligned} \Upsilon &= p_2 \left(\frac{D}{2p_1} + \frac{1}{M} \right) \phi^2 \left(a_{1,2}^{(2)} + b_{1,2}^{(2)} + d_{1,2}^{(2)} + e_{1,2}^{(2)} \right) \\ &\quad - \frac{1}{4}\alpha_c \left(1 + \frac{p_1 M}{D} \right) \left(a_{1,2}^{(1)} + b_{1,2}^{(1)} + d_{1,2}^{(1)} + e_{1,2}^{(1)} \right) \phi^2 \\ &\quad + \frac{3}{4}p_3 M^2 \left(\frac{D}{p_1} + M \right) \phi^2. \end{aligned}$$

Appendix E. The values of the parameters \mathbf{a}_i , \mathbf{b}_i , \mathbf{d}_i , $\mathbf{a}_{i,j}$, $\mathbf{b}_{i,j}$, $\mathbf{d}_{i,j}$, and $\mathbf{e}_{i,j}$, as used in Appendices B, C, and D, are

$$\begin{aligned} \mathbf{a}_i &= \begin{cases} \frac{\text{adj}(\mathbf{L}_{(2\phi_i,0)})}{\det(\mathbf{L}_{(2\phi_i,0)})} \frac{1}{2} M \phi_i^2 \begin{pmatrix} 2p_2 M \\ \alpha_c \end{pmatrix} & \text{if } \phi_i > 0, \\ \mathbf{0} & \text{if } \phi_i = 0, \end{cases} \\ \mathbf{b}_i &= \begin{cases} \frac{\text{adj}(\mathbf{L}_{(0,2\psi_i)})}{\det(\mathbf{L}_{(0,2\psi_i)})} \frac{1}{2} M \psi_i^2 \begin{pmatrix} 2p_2 M \\ \alpha_c \end{pmatrix} & \text{if } \psi_i > 0, \\ \mathbf{0} & \text{if } \psi_i = 0, \end{cases} \\ \mathbf{d}_i &= \frac{\text{adj}(\mathbf{L}_{(2\phi_i,2\psi_i)})}{\det(\mathbf{L}_{(2\phi_i,2\psi_i)})} \frac{1}{2} M (\phi_i^2 + \psi_i^2) \begin{pmatrix} 2p_2 M \\ \alpha_c \end{pmatrix}, \end{aligned}$$

and also

$$\begin{aligned} \mathbf{a}_{i,j} &= \frac{\text{adj}(\mathbf{L}_{(\phi_i+\phi_j,\psi_i+\psi_j)})}{\det(\mathbf{L}_{(\phi_i+\phi_j,\psi_i+\psi_j)})} [(\phi_i + \phi_j)^2 + (\psi_i + \psi_j)^2] \frac{1}{4} M \begin{pmatrix} 2p_2 M \\ \alpha_c \end{pmatrix}, \\ \mathbf{b}_{i,j} &= \frac{\text{adj}(\mathbf{L}_{(\phi_i+\phi_j,\psi_i-\psi_j)})}{\det(\mathbf{L}_{(\phi_i+\phi_j,\psi_i-\psi_j)})} [(\phi_i + \phi_j)^2 + (\psi_i - \psi_j)^2] \frac{1}{4} M \begin{pmatrix} 2p_2 M \\ \alpha_c \end{pmatrix}, \\ \mathbf{d}_{i,j} &= \frac{\text{adj}(\mathbf{L}_{(\phi_i-\phi_j,\psi_i+\psi_j)})}{\det(\mathbf{L}_{(\phi_i-\phi_j,\psi_i+\psi_j)})} [(\phi_i - \phi_j)^2 + (\psi_i + \psi_j)^2] \frac{1}{4} M \begin{pmatrix} 2p_2 M \\ \alpha_c \end{pmatrix}, \\ \mathbf{e}_{i,j} &= \frac{\text{adj}(\mathbf{L}_{(\phi_i-\phi_j,\psi_i-\psi_j)})}{\det(\mathbf{L}_{(\phi_i-\phi_j,\psi_i-\psi_j)})} [(\phi_i - \phi_j)^2 + (\psi_i - \psi_j)^2] \frac{1}{4} M \begin{pmatrix} 2p_2 M \\ \alpha_c \end{pmatrix}, \end{aligned}$$

where the operators \det and adj indicate the determinant and adjoint, respectively, of the corresponding matrices. Calculating \mathbf{a}_i , for example, we find that

$$a_i^{(1)} = \frac{2M\phi_i^2(\alpha_c p_1 - 2p_2 DM)}{64D\beta\phi_i^4 + 16(D - \alpha_c p_1)\phi_i^2 + 4D\rho},$$

$$a_i^{(2)} = \frac{-16\alpha_c\beta M\phi_i^4 + 4\alpha_c M(2p_2 M - 1)\phi_i^2 - \alpha_c\rho M}{128D\beta\phi_i^4 + 32(D - \alpha_c p_1)\phi_i^2 + 8D\rho}.$$

Similar forms can be found for $b_{i,j}$, $d_{i,j}$, and $e_{i,j}$.

Acknowledgments. Philip Maini would like to thank the Department of Mathematics, Williams College, Williamstown, Massachusetts, for their hospitality and support. Gerhard Cruywagen would like to thank the Department of Applied Mathematics, University of Washington, Seattle, for their hospitality and support.

REFERENCES

- D.L. BENSON, P.K. MAINI, AND J.A. SHERRATT (1997), *Unravelling the Turing bifurcation using spatially varying diffusion coefficients*, J. Math. Biol., to appear.
- G.C. CRUYWAGEN, P.K. MAINI, AND J.D. MURRAY (1994a), *Travelling waves in a tissue interaction model for skin pattern formation*, J. Math. Biol., 33, pp. 193–210.
- G.C. CRUYWAGEN, P.K. MAINI, AND J.D. MURRAY (1994b), *Bifurcating spatial patterns arising from travelling waves in a tissue interaction model*, Appl. Math. Lett., 7, pp. 63–66.
- G.C. CRUYWAGEN, P.K. MAINI, AND J.D. MURRAY (1992), *Sequential pattern formation in a model for skin morphogenesis*, IMA J. Math. Appl. in Medic. and Biol., 9, pp. 227–248.
- G.C. CRUYWAGEN AND J.D. MURRAY (1992), *On a tissue interaction model for skin pattern formation*, J. Nonlinear Sci., 2, pp. 217–240.
- G.M. EDELMAN (1986), *Cell adhesion molecules in the regulation of animal form and tissue pattern*, Annual Rev. Cell Biol., 2, pp. 81–116.
- M. GRUMET AND G.M. EDELMAN (1988), *Neuron-glia cell adhesion molecule interacts with neurons and astroglia via different binding mechanisms*, J. Cell Biol., 106, pp. 487–503.
- J.P. KEENER (1988), *Principles of Applied Mathematics, Transformation and Approximation*, Addison-Wesley, Reading, MA.
- L.D. LANDAU AND E.M. LIFSHITZ (1970), *Theory of Elasticity*, 2nd ed., Pergamon, New York.
- B.J. MATKOWSKY (1970), *Nonlinear dynamic stability: A formal theory*, SIAM J. Appl. Math., 18, pp. 872–883.
- P.K. MAINI AND J.D. MURRAY (1988), *A nonlinear analysis of a mechanochemical model for biological pattern formation*, SIAM J. Appl. Math., 48, pp. 1064–1072.
- P.K. MAINI, K. J. PAINTER, AND H. N. P. CHAU (1997), *Spatial pattern formation in chemical and biological systems*, Faraday Transactions, to appear.
- J.D. MURRAY (1989), *Mathematical Biology*, Springer-Verlag, Heidelberg.
- J.D. MURRAY AND G.C. CRUYWAGEN (1994), *Threshold bifurcation in tissue interaction models for spatial pattern generation*, Philos. Trans. Roy. Soc. London Ser. A, 347, pp. 661–676.
- J.D. MURRAY, D.C. DEEMING, AND M.W.J. FERGUSON (1990), *Size dependent pigmentation pattern formation in embryos of Alligator Mississippiensis: Time of initiation of pattern generation mechanism*, Proc. Roy. Soc. Ser. B, 239, pp. 279–293.
- J.D. MURRAY AND G.F. OSTER (1984), *Cell traction models for generating pattern and form in morphogenesis*, J. Math. Biol., 19, pp. 265–279.
- B.N. NAGORCKA, V.S. MANORANJAN, AND J.D. MURRAY (1987), *Complex spatial patterns from tissue interactions—an illustrative model*, J. Theoret. Biol., 128, pp. 359–374.
- G.A. NGWA AND P.K. MAINI (1995), *Spatio-temporal patterns in a mechanical model for mesenchymal morphogenesis*, J. Math. Biol, 33, pp. 489–520.
- G.F. OSTER AND J.D. MURRAY (1989), *Pattern formation models and developmental constraints*, J. Exp. Zool., 251, pp. 186–202.
- L.J. SHAW AND J.D. MURRAY (1990), *Model for complex skin patterns*, SIAM J. Appl. Math., 50, pp. 628–648.
- A.M. TURING (1952), *The chemical basis of morphogenesis*, Philos. Trans. Roy. Soc. London Ser. B, 237, pp. 37–72.
- N.K. WESSELLS (1965), *Morphology and proliferation during early feather development*, Dev. Biol., 12, pp. 131–153.
- A.A. WHEELER (1985), *Some aspects of the weakly non-linear theory of the morphological instability*, IMA J. Appl. Math., 35, pp. 131–144.
- E.C. ZEEMAN (1974), *Primary and Secondary Waves in Developmental Biology*, Lectures Math. Life Sci., 4, American Mathematical Society, Providence, RI, pp. 69–161.